AstroSat UVIT Observations of Her X-1

D. A. Leahy , J. Postma, and Y. Chen
Dept. of Physics & Astronomy, University of Calgary, University of Calgary, Calgary, Alberta, T2N 1N4, Canada
Received 2019 October 18; revised 2019 December 17; accepted 2019 December 27; published 2020 January 31

Abstract

An observation of the X-ray binary system Her X-1/HZ Her by the AstroSat UltraViolet Imaging Telescope (UVIT) was carried out in 2018. The observation was taken with the far ultra-violet (FUV) camera of UVIT with the CaF_2 filter (125–175 nm band) and lasted $\simeq 0.6$ of one binary orbit. Her X-1 was in the late main high state at 35 day phase $\simeq 0.20$. Clear orbital modulation of the UVIT light curve is seen, showing egress from eclipse of the neutron star and double-peak shape half an orbital period later. The FUV emission from Her X-1 is shown to arise partly from the accretion disk and partly from the X-ray heated face of Hz Her. We carry out modeling of the system using the Shape code and fit the FUV light curve. New constraints are obtained for the geometric parameters of the tilted and twisted accretion disk around the neutron star, and improvements to the basic disk model are suggested.

Unified Astronomy Thesaurus concepts: Neutron stars (1108); X-ray binary stars (1811)

1. Introduction

Her X-1/HZ Her continues to be a well-studied persistent X-ray binary pulsar. Leahy & Chen (2019) reported spectral analysis of AstroSat Soft X-ray Telescope observations of Her X-1 during low state, turn-on, main high state, and main high during dip. Wolff et al. (2016) applied a radiation-dominated radiative shock model to the main high *NuSTAR* X-ray spectrum of Her X-1 to find physical parameters of the accretion flow. Šimon (2015) compared long-term *RXTE*/ASM X-ray monitoring with AAVSO optical data to show the X-ray main high state fluence is considerably more variable than the optical fluence. Leahy (2015) utilized *RXTE*/PCA X-ray eclipse observations to detect and measure the extended scattering corona in the binary system. The masses and uncertainties of the neutron star (Her X-1, $\sim 1.5\,M_\odot$) and its stellar companion (HZ Her, $\sim 2.3\,M_\odot$) are reviewed in Leahy & Abdallah (2014) and Reynolds et al. (1997).

Her X-1/HZ Her radiates in optical, ultraviolet, EUV, and X-ray bands so allows studies of the system from many different aspects. Systematic variations of the 1.7 day optical light curve (Gerend & Boynton 1976) give strong evidence for a Roche-lobe-filling precessing accretion disk. EUV emission (Leahy & Marshall 1999; Leahy et al. 2000; Leahy 2003) originates in the inner disk and from the irradiated surface of HZ Her. Accretion of matter onto the rotating neutron star produces X-rays ($>1\,keV$). The pulsations (Leahy 2004a, 2004b) are determined by the column geometry and by light-bending in the neutron star's gravity.

Both the flux and the pulse shapes exhibit a 35 day cycle. The systematic changes are caused by the precessing accretion disk in the system (Scott et al. 2000). The disk partially or fully blocks the line of sight (LOS) to the neutron star during the short high state, turn-on, and low state. The geometry of the accretion disk has been characterized by modeling the 35 day cycle (Scott & Leahy 1999; Leahy 2002, 2004c and Leahy & Igna 2011). The accretion stream from HZ Her to the disk was shown to cause the well-known X-ray absorption dips (Igna & Leahy 2011, 2012).

The atmosphere of HZ Her causes X-ray absorption detected during eclipse ingresses and egresses (Day et al. 1988; Leahy &

Yoshida 1995). X-rays reflected off the companion star are detected during the low state and short high state (Abdallah & Leahy 2015). Timing of the main high ingresses and egresses enabled accurate determination of the radius of HZ Her (Leahy & Abdallah 2014). Overall, the regular time-variations in Her X-1 are understood as caused by the geometry of the system, such as the Roche-lobe filling companion star and the accretion disk and stream.

AstroSat (Singh et al. 2014), was launched on 2015 September 28. It has four instruments that obtain simultaneous observations over near and far-ultraviolet (NUV and FUV) with the UVIT instrument, and soft through hard X-rays with the SXT, LAXPC and CZTI instruments. UVIT and its calibration are described in Tandon et al. (2017), Postma et al. (2011) and references therein. SXT covers the energy range 0.3–8 keV and is described in Singh et al. (2017). LAXPC is a large area proportional counter, sensitive to the 3–100 keV band, and is described in Yadav et al. (2016). CZTI is a coded mask imager in the 25–150 keV band, and is described in Bhalerao et al. (2017).

Here we analyze the AstroSat UVIT observations of Her X-1. In Section 2 we describe the observations and data analysis to obtain the FUV light curve of Her X-1. In Section 3, we discuss the possible physical mechanisms for the FUV emission and carry out modeling of the FUV light curve. We discuss the modeling results and summarize the work in Sections 4 and 5.

2. Observations

The observations of Her X-1 with UVIT were carried out as part of AstroSat observing session T02. The observation dates were 2018 September 21 and 22. Her X-1 was observed in X-ray bands during T02 with SXT, LAXPC and CZT. The analysis of the X-ray data will be combined with analysis of the X-ray data from the other AstroSat observing sessions of Her X-1 (A02 and A03) for which UVIT was not operating. This will allow a more comprehensive view of the X-ray behavior of Her X-1 and will be reported on in separate work.

The Her X-1 orbital phase was determined using the ephemeris of Staubert et al. (2009). To determine the 35 day

Table 1
UVIT Observations of Her X-1

MJD (start)	MJD (end)	Exposure	$\phi_{\mathrm{orb},1}$[a]	$\phi_{\mathrm{orb},2}$[a]	$\phi_{35\ \mathrm{day},1}$[a]	$\phi_{35\ \mathrm{day},2}$[a]
58381.87	58382.81	8795 s	0.0659	0.625	0.18	0.21

Note.
[a] 1 and 2 indicate observation start and end for orbital phase, ϕ_{orb}, and 35 day phase, $\phi_{35\ \mathrm{day}}$.

phase, the *SWIFT*/BAT Hard X-ray Transient Monitor archive data (Krimm et al. 2013) of Her X-1 were analyzed. Light curves were created for several 35 day cycles around the time of the AstroSat UVIT observation. *Swift*/BAT did not record any data for Her X-1 for the 7 day interval (MJD58371 to MJD58377) covering turn-on for the current 35 day cycle of interest. The previous two cycle turn-ons were at MJD58307.5 and MJD58342.0 within 0.5 day, and the following two cycle turn-ons were at MJD58410.5 and MJD58446.5. Using the mean 35 day cycle length of 34.7 days (Leahy & Igna 2010) yields turn-on estimate times of MJD58376.7, using the previous cycle, or MJD58375.8, using the following cycle. If instead we take the half-way point between the previous and following turn-ons, we obtain a cycle length of 34.25 days and turn-on at MJD58376.25. We take the latter as the best estimate, with uncertainty of $\simeq 1$ day. Then the start of the UVIT observation at MJD58381.87 corresponds to 35 day phase 0.18 with uncertainty 0.03.

Table 1 summarizes the observation parameters. Her X-1 is in the late main high state. The *Swift*/BAT light curve of Her X-1 for the remainder of the high state of the 35 day cycle containing the UVIT observation is shown in Figure 1 (top panel). The shape of the BAT light curve was compared to the *RXTE* average light curve, shown in Figure 2 of Leahy & Igna (2011). This gives an estimate of 35 day phase of 0.15–0.25, consistent with the BAT estimates.

In the lower panel of Figure 1 we show the light curve from the Large Area Proportional Counter (LAXPC) Unit 02 on AstroSat. Comparison of this to *RXTE*/PCA light curves (Leahy & Igna 2011) shows that Her X-1 has the expected eclipse egress at orbital phase 0.07, and that Her X-1 is in a normal late main high state, with a few dips during the observation.

2.1. FUV Light Curve

The FUV light curve of Her X-1 was constructed as follows. The basic data from the UVIT CMOS detectors was read out at 29 frames/s for both FUV and VIS (350–430 nm) detectors. The images of Her X-1 from the VIS channel were used to correct for satellite pointing drift. The resulting time resolution of the drift-corrected FUV images was the full exposure time during one satellite orbit. This exposure time ranged from 151 s to 832 s with mean of 586 s. For each of the drift-corrected images, the raw counts value from Her X-1 was measured by the growth-curve method (e.g., Tandon et al. 2017). In this method, the counts inside a circle of radius r (in pixels) is extracted as a function of r, then the resulting curve is fit by the line $f(r) = a \times \pi r^2 + b$. The constant a gives the background counts per pixel and the constant b gives the source counts, assuming no other sources inside the circle of largest r. In the FUV channel of UVIT, the image of Her X-1 has no contaminating sources within $5'$, so the growth-curve method works well. The raw count rate is high enough, 9–64 c s^{-1}, that
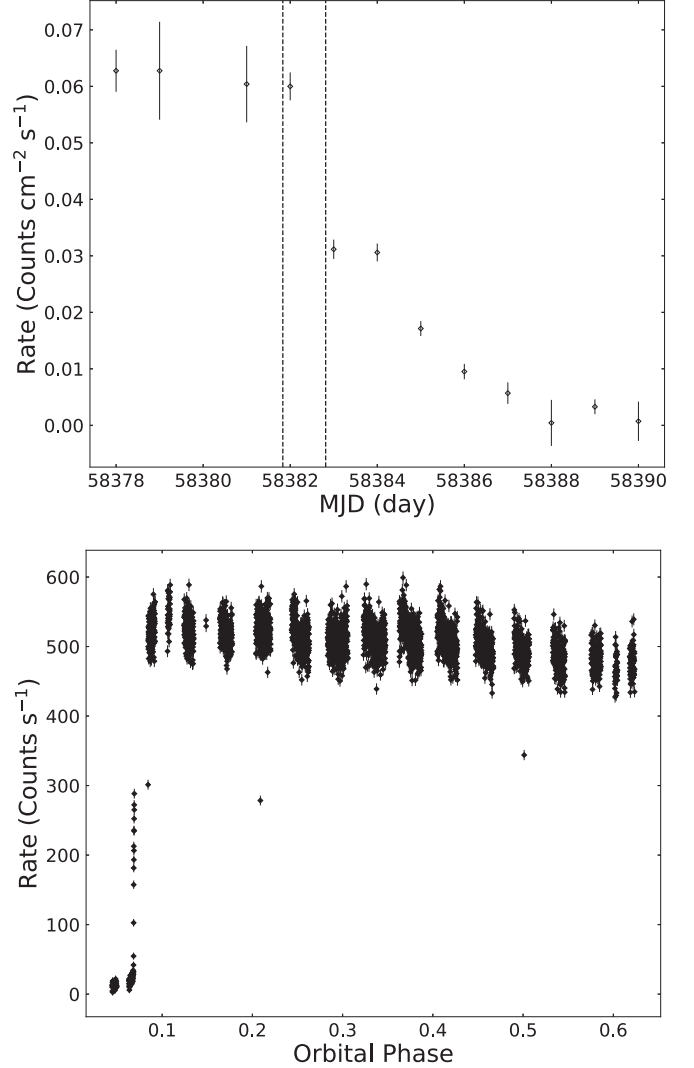
Figure 1. Top: *Swift*/BAT light curve of Her X-1 for 12 days around the time of the AstroSAT T02 observation of Her X-1. The time period of the AstroSAT observation is indicated by the vertical dashed lines. Bottom: LAXPC 3–80 keV light curve of Her X-1 during the AstroSAT observation, with egress from eclipse at orbital phase 0.07.

there is significant probability of more than one event being recorded in the same CCD resolution element within one frame of length $(1/29)$ s. Thus the raw count rate and the error in count rate were corrected for saturation, using the procedure described in Postma & Leahy (2017).

The resulting UVIT FUV light of Her X-1 is shown in Figure 2 (top panel). The mean FUV count rate of Her X-1 over the UVIT observation is 42.8 ct s^{-1}. This translates to an observed flux of $f_\lambda = 1.32 \times 10^{-13}$ erg cm^{-2} s^{-1} A^{-1}, or $f = 6.6 \times 10^{-11}$ erg cm^{-2} s^{-1} integrated over the FUV CaF2 filter bandbass.
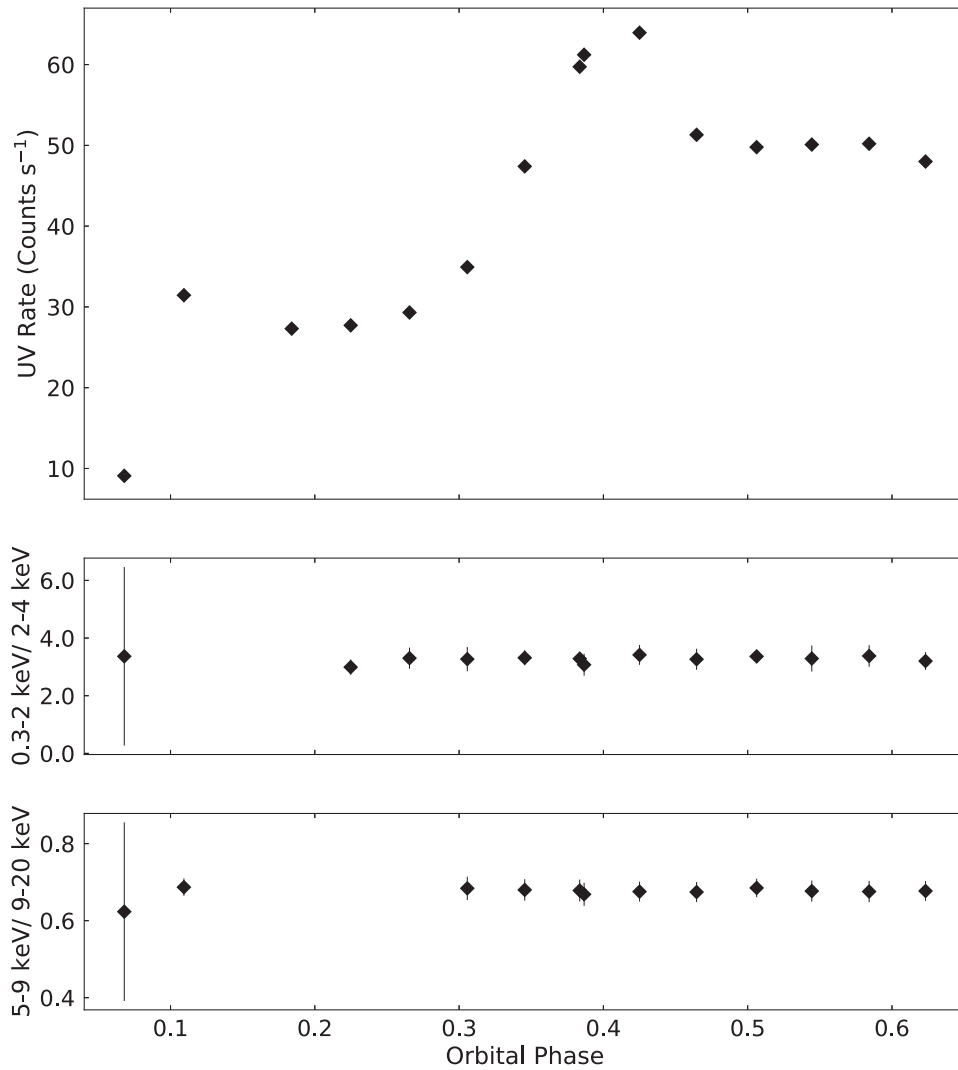
Figure 2. Top: UVIT CaF$_2$-filter (125–175 nm band) T02 light curve. Middle: SXT softness ratio (0.3–2 keV/2–4 keV) with the same time bins as the UVIT light curve. Bottom: LAXPC20 softness ratio (5–9 keV/9–20 keV) with the same time bins as the UVIT light curve. The X-ray softness ratios are constant during the UVIT observation.

The lower two panels of Figure 2 show the X-ray softness ratios from the Soft X-ray Telescope on AstroSat and from the LAXPC. The constancy of the softness ratios shows that the X-ray spectrum is essentially constant for the UVIT observation. Together with the LAXPC light curve (lower panel of Figure 1), it is seen that the X-ray emission from Her X-1 is essentially constant, except during eclipse egress, for the UVIT observation.

3. Model Fitting and Results

The Her X-1 system is well studied in X-rays and optical, so the basic properties of the X-ray source, accretion disk, and companion star are known (e.g., Leahy & Igna 2011 and Leahy & Abdallah 2014). The source of the FUV emission is not as well understood, so we review the emission mechanisms for FUV for the Her X-1 system. After the probable mechanism for the observed FUV flux is established, a detailed model is constructed and applied to the UVIT data.

3.1. Source of the UV Emission

The neutron star accretion column emits strongly in the $\sim$1–30 keV band with bolometric luminosity $\sim$4 $\times$ 10^{37} erg s^{-1}. Approximating this as a 5 keV blackbody yields a Rayleigh–Jeans tail with flux in the FUV band of 2.1×10^{-18} erg cm^{-2} s^{-1}, much smaller than the detected flux. Any accretion column emission Thompson-scattered from the accretion disk or from the face of HZ Her will be of smaller intensity than the above flux, so will be negligible.

The accretion column radiation heats the neutron star surface, which then radiates at a lower temperature. The area heated is of the order of a few km^2, compared to the area of the accretion column of order 0.1 km^2 (e.g., Leahy 2004b). This yields a heated surface temperature of $\sim$1–2 keV, and a Rayleigh–Jeans tail in the UVIT CaF2 filter of 1×10^{-18} erg cm^{-2} s^{-1}, which is negligible compared to the observed flux.

For the most recent summary of the X-ray spectrum of Her X-1 see Leahy & Chen (2019). The X-ray spectrum has a 0.1 keV blackbody component (e.g., Oosterbroek et al. 2000), which comes from the inner surface of the accretion disk. The blackbody has an area of $\simeq$4.5 $\times$ 10^6 km^2. In the UVIT CaF2

filter, the resulting flux is $2.8 \times 10^{-14} \, \mathrm{erg \, cm^{-2} \, s^{-1}}$, less than 0.001 of the observed flux.

The accretion disk is heated by dissipation of energy as the accreted mass moves to lower gravitational potential on its journey through the disk. To obtain a luminosity estimate, we use the α-disk model of Shakura & Sunyaev (1973) and adopt a neutron star mass of $1.5 M_\odot$ and radius of 11 km (Leahy 2004b). The input mass accretion rate from the observed bolometric X-ray luminosity is $\simeq 4 \times 10^{17} \, \mathrm{gm \, s^{-1}}$. Using $\alpha = 0.1$, the temperature of the disk versus radius is found. The temperature depends on $\alpha^{-0.2}$, so is not highly sensitive to the assumed α. Integrating over the disk, the luminosity and hence flux in the UVIT CaF2 filter is estimated as $\simeq 3 \times 10^{-11} \, \mathrm{erg \, cm^{-2} \, s^{-1}}$. This is comparable to the observed FUV flux. However during one orbit of Her X-1, the observed disk flux is not expected to be variable except for the eclipse of the disk by HZ Her near orbital phase 0. Thus another source of FUV emission is needed.

One FUV emission mechanism is the reradiation of incident X-ray flux by the side of HZ Her facing the neutron star. The optical, UV, and EUV emission from HZ Her have been discussed previously: for a summary of the EUV emission and of previous work see Leahy (2003). EUV emission from Her X-1 was observed by the *Extreme Ultraviolet Explorer* (*EUVE*) Deep Survey Spectrometer (DS) during Her X-1 low states in 1993–1997. This *EUVE*-DS emission showed orbital modulations which were modeled by Leahy (2003) using a combination of emission from the heated face of HZ Her and a simplified disk emission component. The HZ Her heated face component was calculated using an analytic model for the variable shadow of the accretion disk on HZ Her. An *EUVE*-DS anomalous low-state observation in 1999 was compared to simultaneous *RXTE*/PCA observations by Leahy & Dupuis (2010). The lack of *EUVE*-DS modulation was attributed to the anomalous state of the accretion disk, with the disk geometry changed so that the X-ray flux heating of HZ Her was significantly depressed compared to normal.

To estimate the FUV emission from the heated face of HZ Her, we approximate the absorption efficiency of X-rays as 0.5 and the fraction of the front face of HZ Her that is illuminated by X-rays as 0.5. The known system geometry then gives the X-ray heating luminosity of HZ Her. Taking the reradiation as blackbody yields the temperature of the heated face as $T_{\mathrm{heat}} = 1.6 \times 10^4$ K. This is in good agreement with observations (Cheng et al. 1995). The area and temperature of the blackbody emission yield a UVIT CaF2 flux of $\simeq 3.7 \times 10^{-11} \, \mathrm{erg \, cm^{-2} \, s^{-1}}$.

Thus the two expected contributors to the observed UVIT FUV flux are the accretion disk emission and the emission from the heated face of HZ Her. Next we discuss construction of an emission model and fitting that model to the UVIT FUV light curve.

3.2. Her X-1 System Geometry

The Her X-1 system geometry is discussed in Leahy & Abdallah (2014), where existing constraints on the orbit from X-ray timing were combined with new constraints from precise timing of X-ray eclipses observed by the *RXTE*/PCA. Precise values of masses of the neutron star and HZ Her, of semimajor axis, and companion radius depend on the orbital inclination. The inclination is limited to be in the range $>80°$ to $<90°$ to produce the 35 day cycle (Scott et al. 2000; Leahy 2002). The

other parameter (see Table 3 of Leahy & Abdallah 2014) can be taken as either the mass ratio, q, or the amplitude of the velocity of HZ Her, K_c. Here we take the parameter as $q = M_x/M_c$ with neutron star mass $M_x = 1.5 M_\odot$ and HZ Her mass $M_c = 2.3 M_\odot$. This is consistent with the observed limits on K_c.

The upper inclination limit of 90° is not allowed by the observed 35 day cycle. Although precise constraints on inclination have not yet been determined, most previous work has either used 85° or a range of 82°.5–87°.5. In this study, we use the latter range and include the dependence of geometric parameters (e.g., semimajor axis, HZ Her radius, outer disk radius) on inclination. With inclination as a variable, we can test whether the UVIT data can constrain the inclination.

HZ Her is taken as Roche-lobe filling (e.g., Leahy & Leahy 2015). We verified that to three digits, this agrees with the radii measured by Leahy & Abdallah (2014) for different inclinations.

3.3. Accretion Disk Geometry

The accretion disk model is taken as a twisted and tilted disk, also referred to as a warped disk (e.g., Wijers & Pringle 1999), consisting of a continuous series of rings each with its own twist and tilt. The twist and tilt are smooth functions of radius, which results in the warped disk shape. The twist and tilt parameters of a single ring are illustrated in the first panel of Figure 3. The twist is the angle of the line of nodes from the projection of the LOS onto the orbital plane, and is measured in the orbital plane. The tilt is the angle between the normal to the ring and the normal to the orbital plane.

The disk model is essentially the same model as used to fit the 35 day light curve of Her X-1 by Leahy (2002). In that work the constraints were determined for observer LOS parameters rather than disk geometry parameters.[1] We start with the thin disk geometry illustrated in Figure 2 in the above paper. Later we test the effects of adding a thick highly tilted inner ring as illustrated in their Figure 7. The thick inner ring was added by Leahy (2002) to better fit the 35 day cycle's X-ray light curve. The thick inner ring has small radius (~ 400 km) compared to the outer disk radius ($\sim 2 \times 10^6$ km) but large solid angle as viewed from the neutron star. Thus it can significantly affect the shadow of the accretion disk on HZ Her.

The geometry of the warped disk is specified by taking a tilt angle of the inner ring of the disk from the orbital plane and a tilt angle of the outer ring. Intermediate rings have a tilt that is a linear function versus radius between the inner tilt and the outer tilt. The twist is specified as the change of line-of-nodes (LON) angle for each disk ring with radius. It is taken as a linear function of radius between the inner ring LON angle and the outer ring LON angle.

Assuming a counterclockwise binary orbit (viewed from the north pole of the orbit), the disk rotates clockwise with increasing 35 day phase. The disk LON must increase in a counterclockwise direction with increasing disk radius to be consistent with the observed 35 day cycle (Scott & Leahy 1999; Scott et al. 2000). The reference point for zero LON angle is defined here to be the projection of the observers LOS onto the disk plane. Because we start our model at 35 day phase

---

[1] Additional geometric calculations are required to convert the observer LOS parameters into disk geometry parameters.
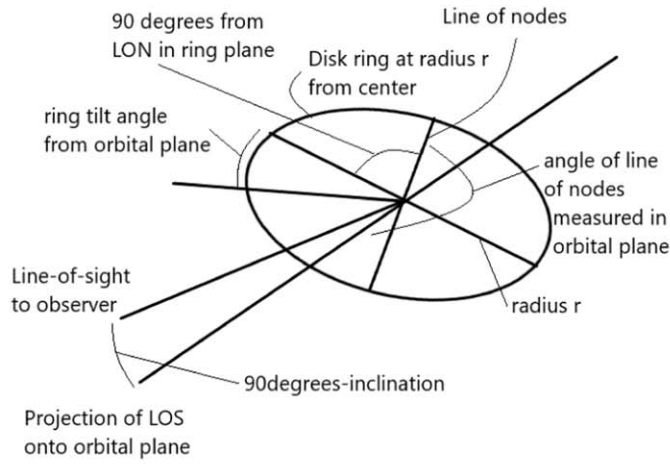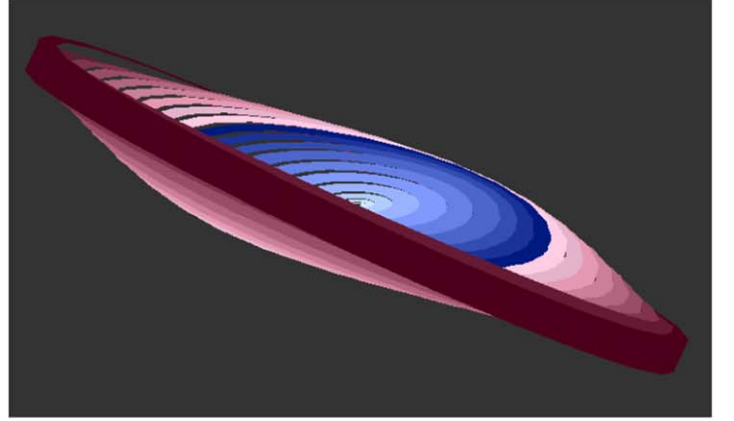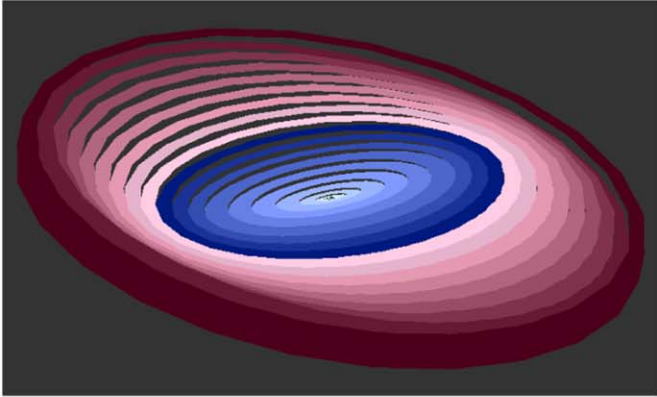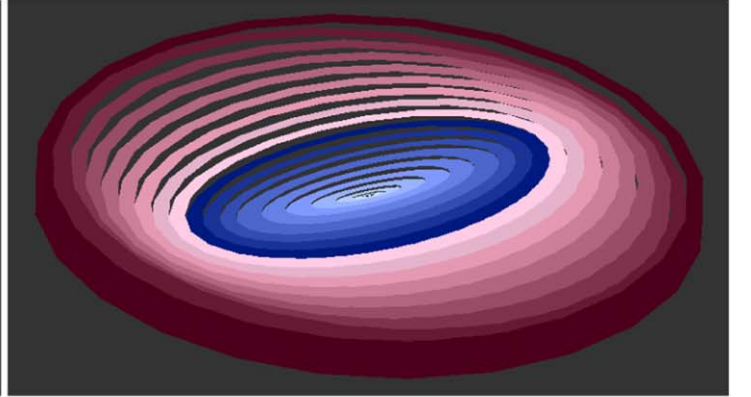
Figure 3. Disk and geometry. Panel (a): geometry of a single circular ring of radius *r* in the disk showing observer line of sight (LOS), ring line-of-nodes (LON) angle and ring tilt. The twisted-tilted disk is constructed from a series of rings of differing radius, tilt, LON and vertical thickness. Panels (b)–(d): filled wireframe model of the disk, consisting of 19 rings with tilt, twist and thickness as linear functions of radius. The disk precession is clockwise with increasing 35 day phase. The line-of-nodes (twist) and tilt parameters for the disk are those given in Table 3 for $i = 85°$. In all three panels, the view is for 85° inclination. For panel (b) 35 day phase is 0; For (c) 35 day phase is 0.18, and for (d) 35 day phase is 0.18 plus one binary orbit, i.e., 0.2286.

$\phi_{35} = 0.18$, the LON angles are referenced to this 35 day phase. The LON angles for any other 35 day phase are obtained by subtracting $(\phi_{35} - 0.18) * 360°$ from the LON angles given here.

The goal here is to calculate the disk emission and the disk shadow on HZ Her. We approximate the disk to have a sharp boundary perpendicular to the local disk normal at height z above the disk plane at $z/r = 0.055$, with *r* the distance from the neutron star. This approximates the increase in thickness with radius expected for an α-disk. Thus the full disk thickness-to-radius ratio h/r is taken as a constant in this model. The twisted-tilted disk geometry is illustrated in the top panel of Figure 3. The orientations of the disk are shown for 35 day phase 0 (main high X-ray turn-on, panel (b)), at 35 day phase 0.18 (panel (c)), which is the time of orbital phase 0 just prior to the UVIT observation, at 35 day phase 0.2286 (panel (d)), which is the 35 day phase for 1.0 binary orbit after the UVIT observation.

In summary, the geometry of the disk has the following parameters: inner and outer radius, r_{in} and r_{out}, inner and outer disk tilt, θ_{in} and θ_{out}, inner and outer LON angles, ϕ_{in} and ϕ_{out},

and disk thickness to radius ratio, h/r. The only parameter for the binary system (semimajor axis a, and Roche-Lobe filled geometry of HZ Her) is system inclination, i.

3.4. Emission Model

The two expected contributions to the FUV light curve of Her X-1 are radiation from the X-ray heated face of HZ Her, and radiation from the disk surface. The system geometry of HZ Her and accretion disk is illustrated in Figure 4 for three different orbital phases. The geometries of the two components are somewhat complex: the Roche-lobe filling star HZ Her, and the tilted and twisted disk. To calculate the emission from the star and the disk we use the radiation transfer code Shape (Steffen & López 2006). This allows construction of user-specified geometries. The system geometry is built up using a set of primitive geometric objects, such as spheres, cones and cylinders, each with its own set of parameters. Exempli gratia for a cone, one specifies location (*x*, *y*, *z*) of the apex, cylinder height, base radius and orientation of the cone axis by two

(a)

(b)

(c)
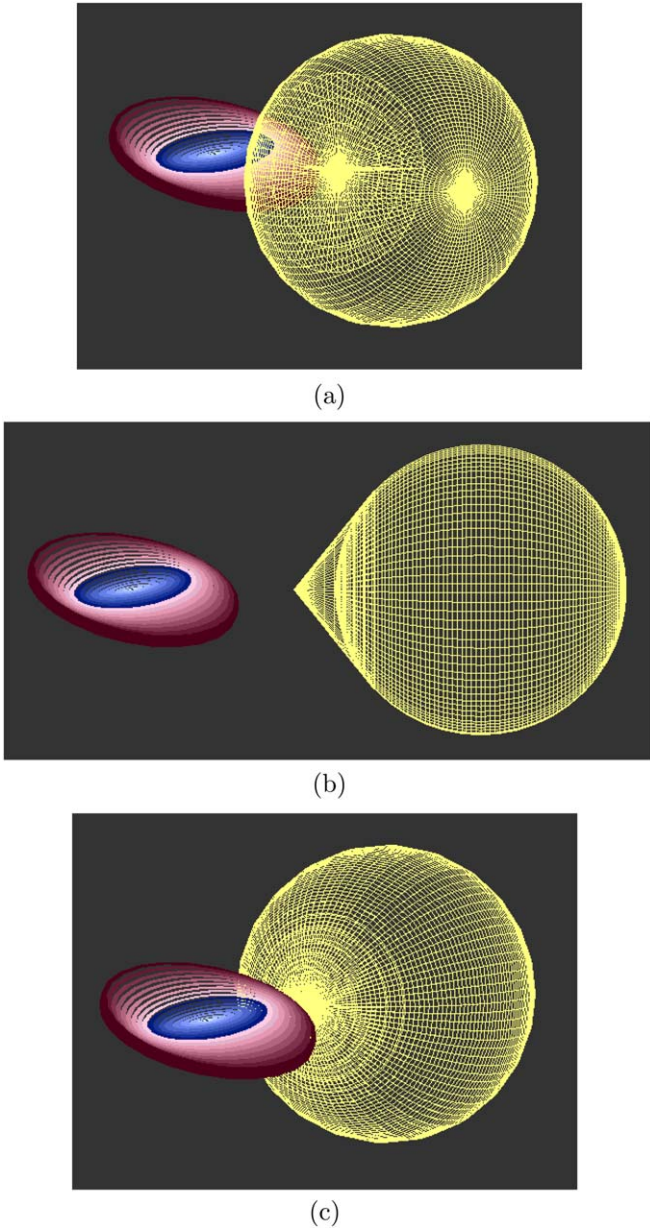
Figure 4. The binary geometry, including the Roche-lobe filling HZ Her and the twisted-tilted disk, is shown for parts of a binary orbit that starts at 35 day phase 0.18. The binary orbit is counterclockwise, opposite the clockwise disk precession. Orbital phase 0.0 is when HZ Her is closest (and neutron star furthest) to the observer. The orbital phases shown are (a) 0.0833; (b) 0.25; and (c) 0.4167. The binary parameters (orbital separation, HZ Her y-radius and L1 point, and disk outer radius) were computed for system inclination of $i = 85°$.

angles. The density of absorbing or emitting particles can be specified by a function of the coordinates.

After the geometry is set and the direction to the observer is set, Shape carries out a ray-tracing calculation; i.e., a large number of rays are cast in all directions from emitters in the system, with the energies of the rays distributed according to a user-specified spectrum. Each ray is traced until it is lost (is absorbed or leaves the calculation volume in a direction not toward the observer) or is received by the observer with a small angle from the LOS, specified in Shape by the field of view. The directions of received rays are stored to create an image in a chosen energy band. The total flux seen by the observer is obtained by integrating surface brightness over the simulated

image. In our case, we calculate the simulated image and flux for the UVIT FUV CaF2 filter band of 125–175 nm.

To approximate the continuous twisted-tilted disk in Shape, we used a set of n adjacent cylindrical rings with label k, $k = 0$, $1 \ldots n - 1$. The inner radius and outer radius of the innermost ring are r_0 and r_1, and the inner radius and outer radius of the outermost ring are r_{n-1} and r_n; i.e., the inner disk radius is $r_{in} = r_0$ and the outer disk radius is $r_{out} = r_n$. The outer radius was taken to be $0.7 \times d_{L1,X}$ with $d_{L1,X}$ the distance from the neutron star to the L1 point. Each ring has its own tilt, twist and thickness, which are specified as linear functions of radius. Writing the tilt angle as θ, the twist angle as ϕ, and the full disk thickness as h, we have

$$\theta_k = \theta_{in} + (r_k - r_{in})/(r_{out} - r_{in}) \times (\theta_{out} - \theta_{in}) \tag{1}$$

$$\phi_k = \phi_{in} + (r_k - r_{in})/(r_{out} - r_{in}) \times (\phi_{out} - \phi_{in}) \tag{2}$$

$$h_k = r_k \times h/r. \tag{3}$$

For model fitting, the thickness to radius ratio, h/r, r_{in}, and r_{out} are taken as a fixed constants and the parameters θ_{in}, θ_{out}, ϕ_{in}, and ϕ_{out} are free parameters.

The shape of HZ Her was approximated as a sphere with radius equal to the y-radius of a Roche-lobe filling surface, with an added conical cap tangent to the sphere and with apex at the L1 point. The difference between the approximate shape and the exact Roche-lobe filling shape was verified to be small in all directions.

Shape uses a finite three-dimensional rectangular grid. To obtain more accurate results, the disk UV emission and HZ Her UV emission versus orbital phase were calculated with separate models. For the disk UV emission, the area of the emission region is important so we used a small inner disk radius ($r_{in} = 0.025 \times r_{out}$), to have a large number of cells covering the disk and to preserve the area. For the small radius inner rings, the mapping onto the rectangular grid means the circular shape of inner rings is not well preserved. For the disk emission calculation, we used 19 disk rings. The disk surface was taken as an optically thick layer with blackbody emission with variable temperature with radius, given by the α-disk model ($T(r) \propto r^{-3/4}$). The disk emissivity was enabled and photo-electric absorption of radiation by HZ Her was enabled, but the heating of the face of HZ Her (thus radiation from HZ Her) was turned off.

To calculate the radiation emitted from the heated face of HZ Her, it is important to model accurately the shape of disk shadow, which depends on the solid angle subtended by the disk at the neutron star. Thus we used a large inner disk radius ($r_{in} = 0.30 \times r_{out}$) so the mapping of the innermost circular ring onto the rectangular calculation grid preserves the shape of the disk shadow. For the disk shadow/HZ Her calculation we used 13 disk rings. For the HZ Her emission calculation, heating of HZ Her by X-rays from the neutron star was included, photoelectric absorption of radiation by the disk was enabled and the blackbody emission from the disk was turned off.

Example images of the heated face of HZ Her seen by the observer at different orbital phases are shown in Figure 5. Because of the asymmetry inherent in the twisted-tilted disk, the illumination of HZ Her changes with orbital phase. At 35 day phase 0.18 the illumination is higher before orbital
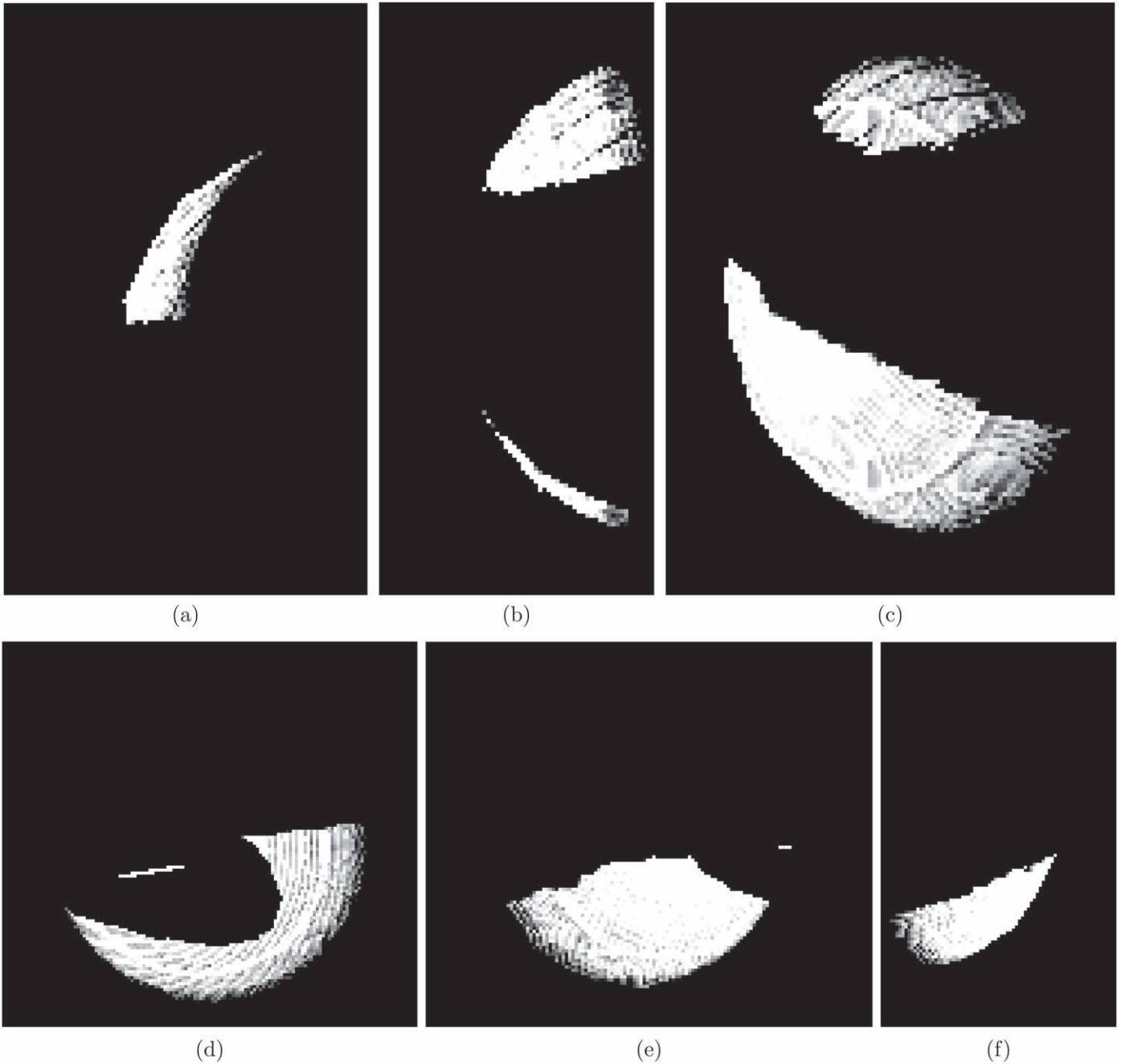
Figure 5. Shape simulated images of the FUV radiation (125–175 nm band) emitted from the X-ray illuminated surface of HZ Her. The images are created from light rays leaving the face of HZ Her toward the observer on Earth at orbital inclination of 85°. The orbital phases shown are (a) 0.175, (b) 0.275, (c) 0.375, (d) 0.475, (e) 0.575, and (f) 0.675. The field of view has been adjusted in each panel and can be found using the radius for HZ Her of 2.7×10^6 km. The limb of HZ Her and the broad horizontal band of the disk shadow on HZ Her are seen as dark areas in all panels (and most clearly seen in panel (c)). The disk occultation of the emission from HZ Her is seen as an elliptical dark area in panels (d) and (e). The brightness scale is logarithmic. Small-scale artifacts are seen in the image which are caused by the projection of the stellar surface onto a rectangular calculation grid.

phase 0.5 than after orbital phase 0.5. There are two effects visible for the observer at 5° above the orbital plane. The disk shadow of the illuminating X-rays from the neutron star is a broad band. The second effect is the disk occultation of UV emission from HZ Her on its way to the observer. This is seen in panels (d) and (e) of Figure 5 as the elliptical dark region.

3.5. Model Fitting

To fit the observed UVIT light curve, we calculated simulated orbital light curves of emission from HZ Her and from the disk. The orbital light curve was calculated at 40 different orbital phases, i.e., 40 different orientations of the system separated by 9° rotations about the system orbital axis. Cubic spline interpolation was used to obtain the light curve at orbital phases intermediately between the calculated phases.

Shape uses ray-tracing to calculate the light curve for a given geometry, and as the complexity of the geometry increases, the computation time increases accordingly. For 13 rings, the computation time for one model orbital light curve (one set of parameters) was between ~10 and ~40 minutes. Running a multi-dimensional parameter grid of ~500 models took a few
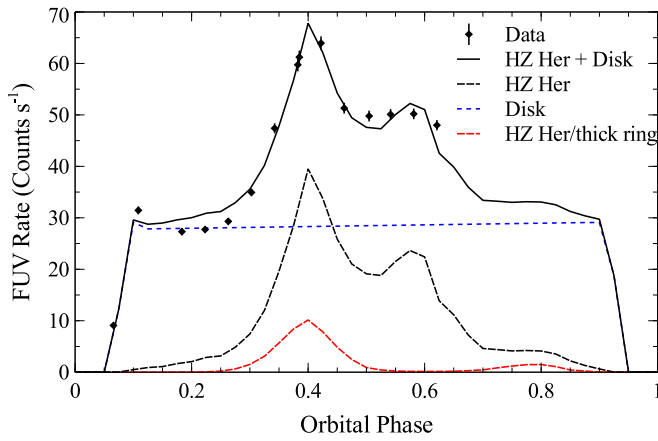
Figure 6. UVIT light curve of Her X-1 (diamonds) and Model A FUV light curve fit (solid line). The model consists of radiation from the heated surface of HZ Her (dashed line) plus radiation from the accretion disk surface (dotted line). Both model components are eclipsed by HZ Her between orbital phases $\simeq 0.93$ and 0.07. For comparison, the radiation from HZ Her for the case of disk with thick inner ring is shown in red.

hundred hours of computation time. The current model uses a rectangular 3D computational grid of 256^3 points (256 in each of x, y, and z dimensions). The projection of the curved surface of HZ Her onto the rectangular grid results in small-scale artifacts. These can be seen as small-scale ripples on the face of HZ Her in Figure 5. The artifacts can be reduced by running a higher resolution calculation. We tested a 512^3 grid, and found that it reduces the artifacts at the expense of eight times longer computation time. The increase to a 512^3 grid resulted in a negligible change in the total calculated flux from HZ Her. Thus we used the 256^3 grid for the model fits to the UVIT light curve.

First we consider disk emission light curves. The normalization is sensitive to the value of normalization for the α-disk model, and the shape is approximately constant outside of the times that the disk is being eclipsed by HZ Her. The disk rotates only a small angle over one orbital period, i.e., the disk rotates once per 35 days or $17°.5$ during an orbital period of 1.7 days. Over the UVIT observation of 0.65 orbits, the disk rotates just $11°.3$. In our first set of models (called Model A), we ignored the disk rotation. Later (Model B) we include disk rotation during the UVIT observation. Figure 6 shows the UVIT data compared to the disk emission component, the HZ Her emission component and their sum. There is only one UVIT data point during eclipse egress, so that the current UVIT data are not sensitive to the eclipse of the disk emission. More observations around the time of eclipse are needed to test the disk emission component.

We carried out the following procedure: calculate the disk emission light curve for fiducial disk parameters; fit the disk emission plus HZ Her emission to the UVIT data with variable parameters for the HZ Her emission; use the best-fit parameters from the HZ Her emission model to recalculate the disk emission; and refit the disk emission plus HZ Her emission to the UVIT data to verify the final best fit. We use the standard definition of χ^2,

$$\chi^2(\{p_k\}) = \sum_{i=1}^{N} (\text{data}_i - \text{model}(t_i, \{p_k\}))^2 / \text{err}_i^2 \qquad (4)$$

with N = number of data points, data_i is the count rate of point at time t_i, err_i is the error in count rate of point i, and $\text{model}(t_i,$

$\{p_k\})$ is the model at time t_i, which depends on the parameter set $\{p_k\}$. For a good fit, the mean expected χ^2 is $N - m$, with m the number of free model parameters. We verified that averaging the Shape calculated light curve over the UVIT duration of each data point (~ 0.003 in orbital phase), made no significant difference to the fitting (change in $\chi^2 < 1.0$).

For fitting Model A, the HZ Her emission models were calculated in Shape for a grid of four smoothly adjusted parameters (inner and outer disk LON angles and inner and outer disk tilt angles), and for three different system inclinations (see Table 2), effectively five free parameters. The fixed system parameters were mass of the neutron star, M_X, the mass of HZ Her, M_c, the radius of HZ Her R_c (in units of semimajor axis a), the outer disk radius (in units of the distance from the neutron star to the L1 Lagrange point), and the disk thickness-to-radius ratio, h/r. a, R_c, and outer disk radius were calculated for each system inclination. The fixed and variable parameters are given in Table 2.

The second data point at orbital phase 0.1 was high compared to all models in our initial fits. Thus we omit that data point from the χ^2 calculation in subsequent fits. Essentially we are not modeling that point, but ascribe the high data value to an extra spatially small and un-modeled system component, such as the accretion stream. The results of fitting Model A are summarized in Table 2. We give the best fit for inclinations of $82°.5$, $85°$, and $87°.5$. The formal uncertainty values for each parameter were found using $\Delta\chi^2 = 4$ (2σ for varying one parameter). The formal uncertainties for twist and tilt angles, in brackets beside each parameter in Table 2, are $\simeq 4°–5°$. The fitting shows that we cannot constrain the inclination ($\Delta\chi^2 \simeq 2$ for $82°.5$ and $85°$ compared to $87°.5$). The best-fit Model A for $85°$ inclination is compared to the UVIT data in Figure 6. Model A gives an overall shape similar to the observed FUV light curve of Her X-1. The peak at orbital phase 0.4 is well fit but the rise (orbital phase 0.13–0.3) and the bump near orbital phase 0.6 are not well fit by Model A.

The best-fit χ^2 is significantly higher than statistically acceptable. This likely means that we are underestimating the parameter uncertainties, primarily because a more complete model likely has parameters partially degenerate with the current fit parameters; i.e., a model with more parameters results in a larger range in $\Delta\chi^2$ for a given confidence range (for a more complete discussion see, e.g., Chapter 14 of Press et al. 1989). The high χ^2 can be attributed to: the data having very small errors; and the model missing some statistically significant physical components. Later in this section we test three modifications to Model A that could improve the fits and lower χ^2. In the discussion section below we discuss additional physically realistic extensions to the model that are not computed in this study. Here we note that the extra parameters required to describe these components would result in too many parameters compared to the number of data points, thus reduce the ability of the data to distinguish between models. Our focus here is on constraining the primary shape parameters of the accretion disk. With more observations we can justify adding more components to the model and testing them.

The first modification to Model A is a modified disk shape to include a thick highly tilted inner ring, as illustrated in Figure 7 of Leahy (2002). The inner ring has a negligible affect on the UV emission from the disk, but significantly affects the shadow of the disk on HZ Her. We added a Thompson-scattering region around the central neutron star so that the central source

Table 2
Parameters of Models for UV Light Curve of Her X-1

Fixed Parameters[a]:					
M_X	M_c	a	R_c[b]	Disk Radius[c]	Disk h/r[d]
$1.5M_\odot$	$2.3M_\odot$	$a(i)$	$0.414a(i)$	$0.7d_{L1,X}(i)$	0.11

Best-fit Parameters: Model A[e]						
Inclination(i)	Inner LON[f]	Outer LON	Inner tilt	Outer tilt	χ^2	χ^2_{red}
82°.5 (fixed)	21° (19–24)	132° (129–134)	10° (8–12)	23° (20–25)	203.2	20.3
85° (fixed)	21° (18–23)	131° (128–133)	11° (9.5–12)	24° (22–26)	203.7	20.4
87°.5 (fixed)	19° (17–21)	129° (127–131)	12° (10–14)	26° (24–29)	201.4	20.1

Model B[e]						
Best-fit Parameters: Inclination(i)	Inner LON	Outer LON	Inner tilt	Outer tilt	χ^2	χ^2_{red}
85° (fixed)	26°	136°	10° (fixed)	25° (fixed)	89.7	7.5

Model C[e]						
Parameters: Inclination(i)	Inner LON	Outer LON	Inner/Outer tilt	FWHM	χ^2	χ^2_{red}
85° (fixed)	26°	136°	10°/25° (fixed)	0.08	46.4	4.2

Notes.

[a] M_X is the mass of the neutron star. M_c and R_c are mass and radius HZ Her. a is the semimajor axis. The full set of binary parameters is given in Leahy & Abdallah (2014).

[b] R_c is taken as the y-radius for a Roche-lobe filling star (e.g., see Leahy & Leahy 2015) with mass ratio of the Her X-1 system. For inclination 85° and assumed masses, the radius is 2.714 $R_\odot$.

[c] $d_{L1,X}$ is the distance from the neutron star to the L1 point. For inclination 85° and assumed masses, the disk outer radius is 2.10×10^{11} cm.

[d] h/r is the ratio of the full disk thickness to radius.

[e] Model A has a non-precessing twisted-tilted disk: a full range of parameters was explored. Model B has a precessing twisted-tilted disk: LON angle parameters were explored. Inclination was fixed at 86°, disk tilt was fixed at 10° (inner), 25° (outer). Model C is the same as Model B but in addition is smoothed with a Gaussian with FWHM in orbital phase to simulate a fuzzy disk shadow on HZ Her.

[f] Figure 2 of Leahy (2002) illustrates the definition of the locus of ascending nodes of the disk. The line of ascending nodes rotates counterclockwise with increasing radius in the disk. The reference point here for 0° is the projection onto the disk plane of the observer's line of sight to the neutron star at 35 day phase 0.18.

is extended with a radius $\simeq 0.75$ that of the inner ring, to reproduce the geometry which best fitted the 35 day X-ray light curve by Leahy (2002). The scattering region optical depth was taken as one-third. The resulting light curve from HZ Her did not closely resemble the UVIT light curve, even allowing for variations of the inner-ring parameters from the best-fit values of Leahy (2002). The reason is that the thick inner ring blocks radiation over most of the orbit from the central source, so that most of the time only the extended scattering region illuminates HZ Her and causes HZ Her to re-emit in the FUV band. The calculated model HZ Her emission light curve for the disk with thick inner ring is shown in Figure 6. The thick inner ring results in a main peak versus orbital phase at phase 0.4 and a much weaker peak at orbital phase 0.8. The HZ Her heating intensity is weaker than the thin disk case by a factor of ~ 5, in part because the disk shadow is larger and in part because the unshadowed region of HZ Her is illuminated by the scattered X-rays from the neutron star, instead of the stronger direct X-ray emission.

The second modification to Model A, called Model B, is to include the amount of disk rotation (11°.3, see above) over the duration of the UVIT observation; i.e., as HZ Her orbits the neutron star counterclockwise with a 1.7 day period, we include the disk precession clockwise with a 35 day period. The disk emission in the FUV band is mainly from the inner part of the disk. The change in the visible area of the disk over an orbital period from 35 day phase 0.18–35 day phase 0.2286 is

illustrated in Figure 3 (panels (c) and (d)). There is not much change in the outer areas of the disk but there is a significant changed in the projected area of the inner part of the disk. This results in a significant change in observed FUV flux from the disk. The Shape radiative transfer calculation verifies this, as shown by the line labeled Disk in Figure 7.

We modified the LON angle parameters to obtain a best fit for Model B to the FUV light curve. This best-fit light curve is shown in Figure 7. It shows a much improved fit to the rise over orbital phase 0.15–0.3 than Model A, but similar disagreement as Model A for the bump near orbital phase 0.6. The best-fit parameters are shown in Table 2. The best-fit LON angles are larger, by 5° compared to Model A. The best-fit χ^2 is much improved, decreasing from ~ 203 to 90.

It is physically realistic that the disk surface does not have a sharp edge but rather an atmosphere, so that the disk shadow on HZ Her would have a fuzzy edge rather than a sharp edge. Currently this is beyond our ability to model in Shape, so we simulate a fuzzy shadow by convolving the Model B light curve with a Gaussian function with a small FWHM in orbital phase. We call this Model C. We tested a few values and found that a FWHM of 0.08 in orbital phase significantly improves the agreement with the observed FUV light curve. This Model C light curve is shown in Figure 7, labeled HZ Her (smoothed) for the HZ Her emission component and HZ Her+Disk (smoothed) for the total. Model C shows a much improved fit to the bump near orbital phase 0.6, at the expense of a worse fit
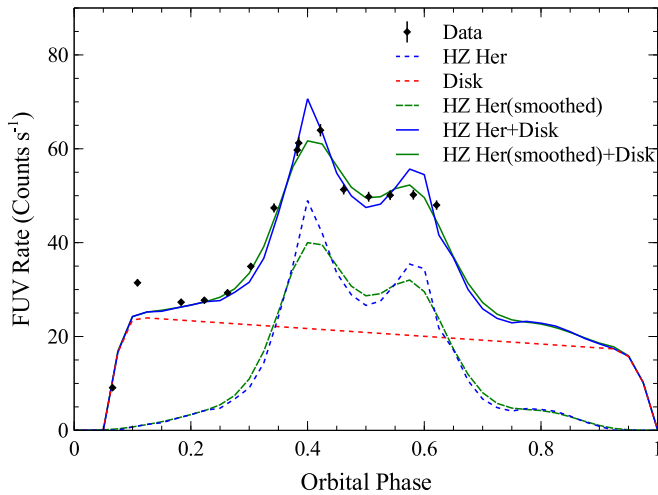
Figure 7. UVIT light curve of Her X-1 (diamonds) with Model B FUV light curve fit (solid blue line) and Model C light curve fit (solid green line). Model B consists of radiation from the heated surface of HZ Her (dashed line) plus radiation from the accretion disk surface (dotted line). The difference from Model A is that Model B includes the disk precession rotation over one orbital period. Model C is the same as Model B but includes smoothing to simulate a fuzzy edge of the disk shadow on HZ Her.

to the peak at orbital phase 0.4. The parameters for Model C are shown in Table 2. The χ^2 is much improved, decreasing from $\sim$90 to 46. We verified that smoothing Model B for parameters different than the Model B best fit did not give as low a χ^2 as that from smoothing the best-fit Model B.

4. Discussion

4.1. Comparison with Previous Work

Gerend & Boynton (1976) show B-band light curves of Her X-1 versus orbital phase for several different 35 day phases. Jurua et al. (2011) show broad band (400–700 nm) light curves for both normal state and for the anomalous low state of Her X-1. The disk shadow model for the B-band light curves of Gerend & Boynton (1976) used a flat and thick tilted disk (see their Figure 3) which precesses with a 35 day period. This model reproduces the main features of the B-band light curves, but it is known to be inconsistent with the 35 day cycle (e.g., Scott et al. 2000). The 35 day X-ray light curve requires a twisted-tilted disk.

Our best-fit model uses the thin tilted-twisted disk model from Leahy (2002; shown earlier in Leahy et al. 2000). The thick inner ring disk model of Leahy (2002) does not fit the FUV light curve thus is conclusively ruled out with the current UVIT data. The thick inner ring was introduced to better reproduce the shape of the short high part of the 35 day X-ray cycle (Figure 4 of Leahy 2002). This means that the geometry of the inner disk is not yet understood nor correctly modeled. Joint fitting of the X-ray and FUV light curves is likely needed to resolve the question of what is the structure of the inner disk.

4.2. Additional Model Components

Our emission model for the thin disk case with geometry from Leahy (2002) fits well the overall shape of the UVIT light curve of Her X-1. The high χ^2 indicates that there are statistically significant components which are missing in the model. Expected physical components not included in the current model include the following.

The comparison of X-ray light curve fitting (Leahy 2002) with the current work shows that the inner disk structure is more complex than either the thin disk model or disk-with-thick-inner-ring model. One possibility is that there is a thick inner ring, but the high latitude part of the inner ring is highly ionized rather than cooler and strongly absorbing in X-rays. In that case, the optical depth of the high latitude part could be in a range ($\simeq$0.5) where back-scattering yields enough X-rays for the short high X-ray light curve, yet enough X-rays are transmitted to illuminate HZ Her and yield the FUV light curve. A UVIT observation during short high, when the disk orientation is significantly different, would be of great value in testing the presence of such a structure or an alternate structure.

The accretion stream and its impact point on the disk (Igna & Leahy 2012) are detected in the Her X-1 system in X-rays. The accretion stream modifies the disk shadow on HZ Her in a complex way. As shown in Igna & Leahy (2012), the angular size of the stream viewed from the neutron star would only be large during orbital phases when the accretion stream impacts the disk at small distance from the neutron star.

An electron-scattering corona surrounds the neutron star, as measured by Leahy (2015). This would modify the observed UV emission by Thompson scattering both X-rays illuminating HZ Her and the UV emitted by the disk and by HZ Her, thus effectively smooth the model light curve. The optical depth of the corona is $\simeq$0.01, so that the effective smoothing should be $\sim$0.01. This is a factor of a few less than the differences between the model and the observed light curve, so likely cannot account for the high χ^2 of our fits.

The inner disk is expected to have a surface layer ionized by the X-ray flux from Her X-1, which would result in a smoother edge in the shadow on HZ Her than in the current model. The smoothing caused by electron scattering of the disk surface could be significant, several %, and account for the flatter UVIT light curve around orbital phase 0.5 compared to the model light curve.

We tested a phenomenological smoothing model here, which had the effect of significantly improving the χ^2 of the best-fit unsmoothed Model B above. However the physical effect of scattering by an ionized disk surface and an electron-scattering corona are orbital phase dependent and not the same as a simple smoothing. A detailed system model is required to properly assess these effects.

In principle these additional model components should be included. However, their geometry is not well constrained so it is currently not feasible to constrain these additional model components with the existing AstroSat/UVIT data of 15 data points. Additional FUV observations would allow testing of these additional model components.

5. Conclusions

The current study of Her X-1 supports the precessing disk model (Wijers & Pringle 1999) for the 35 day light curve (Leahy 2002) and for the 35 day cycle of pulse shape changes (Scott et al. 2000), including disk size and shape, inner disk radius and accretion stream geometry. The current thin disk model for the UVIT light curve (Model C) well reproduces the UVIT FUV light curve of Her X-1 at 35 day phase 0.18. We obtained constraints on the tilt and twist parameters of the thin disk with formal 2σ errors of 4°–5° (Table 2). The disk twist and tilt parameters agree with the constraints obtained by Leahy (2002) within errors. However the model is complex,

with several parameters, the model is incomplete, and the amount of FUV data is limited.

In future work, we will carry out and analyze AstroSat/UVIT observations during the short high state. This will allow a test of the current model for the accretion disk in Her X-1 and enable construction of a more complete system plus disk model. Comparison of the more complete model with both FUV and X-ray light curves promises to yield a better understanding of the accretion mechanism in Her X-1.

ORCID iDs

D. A. Leahy ● https://orcid.org/0000-0002-4814-958X

References

Abdallah, M. H., & Leahy, D. A. 2015, MNRAS, 453, 4222
Bhalerao, V., Bhattacharya, D., Vibhute, A., et al. 2017, JApA, 38, 31
Cheng, F. H., Vrtilek, S. D., & Raymond, J. C. 1995, ApJ, 452, 825
Day, C. S. R., Tennant, A. F., & Fabian, A. C. 1988, MNRAS, 231, 69
Gerend, D., & Boynton, P. 1976, ApJ, 209, 652
Igna, C. D., & Leahy, D. A. 2011, MNRAS, 418, 2283
Igna, C. D., & Leahy, D. A. 2012, MNRAS, 425, 8
Jurua, E., Charles, P. A., Still, M., et al. 2011, MNRAS, 418, 437
Krimm, H. A., Holland, S. T., Corbet, R. H. D., et al. 2013, ApJS, 209, 14
Leahy, D. A. 2002, MNRAS, 334, 847
Leahy, D. A. 2003, MNRAS, 342, 446
Leahy, D. A. 2004a, MNRAS, 348, 932
Leahy, D. A. 2004b, ApJ, 613, 517
Leahy, D. A. 2004c, AN, 325, 205
Leahy, D. A. 2015, ApJ, 800, 32
Leahy, D. A., & Abdallah, M. H. 2014, ApJ, 793, 79
Leahy, D. A., & Chen, Y. 2019, ApJ, 871, 152
Leahy, D. A., & Dupuis, J. 2010, ApJ, 715, 897
Leahy, D. A., & Igna, C. 2010, ApJ, 713, 318
Leahy, D. A., & Igna, C. 2011, ApJ, 736, 74
Leahy, D. A., & Leahy, J. C. 2015, ComAC, 2, 4
Leahy, D. A., & Marshall, H. 1999, ApJ, 521, 328
Leahy, D. A., Marshall, H., & Scott, D. M. 2000, ApJ, 542, 446
Leahy, D. A., & Yoshida, A. 1995, MNRAS, 276, 607
Oosterbroek, T., Parmar, A. N., Dal Fiume, D., et al. 2000, A&A, 353, 575
Postma, J., Hutchings, J. B., & Leahy, D. 2011, PASP, 123, 833
Postma, J. E., & Leahy, D. 2017, PASP, 129, 115002
Press, W. H., Flannery, B. P., Teukolsky, S. A., & Vetterling, W. T. 1989, Numerical Recipes in C. The Art of Scientific Computing (Cambridge: Cambridge Univ. Press)
Reynolds, A., Quaintrell, H., Still, M., et al. 1997, MNRAS, 288, 43
Scott, D. M., & Leahy, D. 1999, ApJ, 510, 974
Scott, D. M., Leahy, D. A., & Wilson, R. B. 2000, ApJ, 539, 392
Shakura, N. I., & Sunyaev, R. A. 1973, A&A, 500, 33
Šimon, V. 2015, AJ, 150, 3
Singh, K. P., Stewart, G. C., Westergaard, N. J., et al. 2017, JApA, 38, 29
Singh, K. P., Tandon, S. N., Agrawal, P. C., et al. 2014, Proc. SPIE, 9144E, 1S
Staubert, R., Klochkov, D., & Wilms, J. 2009, A&A, 500, 883
Steffen, W., & López, J. A. 2006, RMxAA, 42, 99
Tandon, S. N., Subramaniam, A., Girish, V., et al. 2017, AJ, 154, 128
Wijers, R. A. M. J., & Pringle, J. E. 1999, MNRAS, 308, 207
Wolff, M. T., Becker, P. A., Gottlieb, A. M., et al. 2016, ApJ, 831, 194
Yadav, J. S., Agrawal, P. C., Antia, H. M., et al. 2016, Proc. SPIE, 9905, 99051D